

## Article

# Reactive Sintering of $\text{Al}_2\text{O}_3\text{-Y}_3\text{Al}_5\text{O}_{12}$ Ceramic Composites Obtained by Direct Ink Writing

Joana Baltazar<sup>1,2</sup>, Manuel Felipe Rodrigues Pais Alves<sup>1</sup>, Claudinei dos Santos<sup>1,3,\*</sup>  and Susana Olhero<sup>1</sup>

<sup>1</sup> Department of Materials and Ceramic Engineering, CICECO—Aveiro Institute of Materials, University of Aveiro, 3810-193 Aveiro, Portugal; joanambaltazar@ua.pt (J.B.); manuel.alves@ua.pt (M.F.R.P.A.); susana.olhero@ua.pt (S.O.)

<sup>2</sup> Centre for Mechanical Technology and Automation (TEMA), Department of Mechanical Engineering, University of Aveiro, 3810-193 Aveiro, Portugal

<sup>3</sup> Materials and Processes Laboratory, Faculty of Technology, Rio de Janeiro State University, FAT-LMP/UERJ, Resende 27537-000, RJ, Brazil

\* Correspondence: claudineisvr@gmail.com; Tel.: +55-02433813889

**Abstract:** The main goal of this work was to obtain dense  $\text{Al}_2\text{O}_3\text{-Y}_3\text{Al}_5\text{O}_{12}$  ceramic composites by reactive sintering of three-dimensional samples, built by direct ink writing from a paste containing a mixture of  $\text{Al}_2\text{O}_3$  and  $\text{Y}_2\text{O}_3$  powders. To obtain a ceramic ink with proper rheological properties for extrusion-based printing, highly pure  $\text{Al}_2\text{O}_3$  and  $\text{Y}_2\text{O}_3$  powders in a percentage–weight ratio of 64:36 was mixed with 0.2 wt% MgO in a total solid loading of 42 vol% in aqueous media, adding carboxymethyl cellulose and polyethyleneimine solution as additives. The dried printed samples were sintered at final temperatures in the range of 1550 °C and 1650 °C; thus, relative densities of  $83.7 \pm 0.8\%$ ,  $95.4 \pm 0.4\%$ , and  $96.5 \pm 0.5\%$  were obtained for 1550 °C, 1600 °C, and 1650 °C, respectively. Rietveld refinement performed on the X-ray diffraction patterns indicated the presence of  $\text{Al}_2\text{O}_3$  (42 to 47%) and  $\text{Y}_3\text{Al}_5\text{O}_{12}$  (58 to 61%) as crystalline phases, while micrographs showed the presence of equiaxial micrometric grains with average sizes of  $1.8 \pm 0.6 \mu\text{m}$ , for both phases and all sintering conditions. Samples sintered at 1600 °C and 1650 °C presented similar average Vickers hardness values of  $14.2 \pm 0.27 \text{ GPa}$  and  $14.5 \pm 0.25 \text{ GPa}$ , respectively. A slight increase in fracture toughness as sintering temperature increases was also stated, consistent with the densification.

**Keywords:**  $\text{Al}_2\text{O}_3\text{-Y}_3\text{Al}_5\text{O}_{12}$  ceramic composite; direct ink writing (DIW); robocasting; reactive sintering; characterizations; mechanical properties



**Citation:** Baltazar, J.; Alves, M.F.R.P.; dos Santos, C.; Olhero, S. Reactive Sintering of  $\text{Al}_2\text{O}_3\text{-Y}_3\text{Al}_5\text{O}_{12}$  Ceramic Composites Obtained by Direct Ink Writing. *Ceramics* **2022**, *5*, 1–12. <https://doi.org/10.3390/ceramics5010001>

Academic Editors: Frank Kern, Andraz Kocjan, Ángela Gallardo-López and Gilbert Fantozzi

Received: 15 November 2021

Accepted: 21 December 2021

Published: 23 December 2021

**Publisher's Note:** MDPI stays neutral with regard to jurisdictional claims in published maps and institutional affiliations.



**Copyright:** © 2021 by the authors. Licensee MDPI, Basel, Switzerland. This article is an open access article distributed under the terms and conditions of the Creative Commons Attribution (CC BY) license (<https://creativecommons.org/licenses/by/4.0/>).

## 1. Introduction

Alumina-based ceramics have been used for several decades in structural applications, due to their excellent dimensional integrity and stability at high temperatures, intrinsic corrosion resistance from their strong ionic chemical bonds, high hardness, and, consequently, high wear resistance [1–3]. However, due to its chemical nature and microstructure, this ceramic is inherently brittle, presenting low flexural strength and fracture toughness [4,5], which precludes its use in applications where strength and reliability are essential.

An unusual strategy used in hard and brittle ceramics to improve some mechanical properties involves the variation of their base composition from the insertion of a second crystalline phase that presents thermal compatibility with the ceramic base matrix, which aims to create a composite [6]. Among several ways commonly used to obtain ceramic composites from physical mixtures of powders, it is necessary to highlight the importance of the development of these mixtures, namely the control certain parameters as powder nature and amount, considering distinct and stable ceramics at elevated temperatures. For example, in the case of  $\text{Al}_2\text{O}_3$  and yttria-stabilized zirconia Y-TZP (composites), zirconia-toughened alumina (ZTA) or alumina-reinforced zirconia ceramics (ATZ, alumina-toughened zirconia) could be attained depending on their proportions [7,8]. In another type of composites, constituent materials can chemically react at elevated temperatures in a

process of phases transformation “in situ”, called “reactive sintering” [9,10], resulting in different crystalline phases after sintering, as, for example, in the binary ceramic system  $\text{Al}_2\text{O}_3\text{-Y}_3\text{O}_2$ , where crystalline phases, such as YAG ( $\text{Y}_3\text{Al}_5\text{O}_{12}$ ), YAP ( $\text{YAlO}_3$ ), or YAM ( $\text{Y}_4\text{Al}_{12}\text{O}_9$ ), can be formed. The new phases formed depend on the composition used as well as on the sintering temperature, inducing changes in the chemical and physical properties of the final material.

Several works [3,11–13] have reported on the development of ceramic composites based on  $\text{Al}_2\text{O}_3$  by reactive sintering. In particular, the non-stoichiometric  $\text{Al}_2\text{O}_3\text{-Y}_2\text{O}_3$ -based system helps to attain successful densification and enhanced mechanical properties. The main responsibility is linked to intermediate phases such as YAP, YAM, and YAG ( $\text{Y}_3\text{Al}_5\text{O}_{12}$ ), which can appear in the  $\text{Al}_2\text{O}_3$  matrix, considerably altering the initial properties of the material, through a good compromise between densification and grain growth. In fact, besides thermal compatibility, these phases are also responsible for a microstructural control, attained at temperatures below 1650 °C, i.e., a usual sintering temperature for  $\text{Al}_2\text{O}_3$  ceramics [14].

Robocasting or direct ink writing (DIW) appear as innovative additive manufacturing techniques for developing structural ceramics with complex shapes [15,16], consisting of a layer-by-layer extrusion deposition of a filament of a ceramic paste (or ink). Printed ceramic 3D components need to be subsequently dried and sintered, similar to the most conventional ceramic fabrication. Although widely successfully used in the manufacture of porous 3D ceramic components as scaffolds for tissue engineering, there are still considerable difficulties in the fabrication of dense structures [17–19]. Some recent studies have demonstrated the viability of this technique to fabricate dense monolithic  $\text{Al}_2\text{O}_3$  ceramics by increasing the number of solids and flowability of the paste, controlling the printing parameters (in-fill patterning), and the sintering cycle to obtain a better debinding/densification ratio [20]. The inherent features to the printing process, namely the inks’ properties determined essentially by the type and amounts of additives, solids loading, particle size distribution and homogeneity of all components, could influence the green particles packing, the drying step and consequently the sintering process. Literature presents already some reports regarding the fabrication of ceramics from composite pastes containing mixtures of powders by additive manufacturing, which may undergo phase transformations and chemical reactions during the sintering cycle (reactive sintering) [3]. Recently, Zhang et al. [21] obtained YAG–Nd-based dense ceramics by robocasting for optical applications using stoichiometric ratios of  $\text{Y}_2\text{O}_3$  and  $\text{Al}_2\text{O}_3$ . Nevertheless, from authors knowledge, the use of direct ink writing to produce composites based on non-stoichiometric powder mixtures of  $\text{Al}_2\text{O}_3$  and  $\text{Y}_2\text{O}_3$  have not yet been reported, with the consequent absence of results related to the inks preparation and their influence on sintering behavior and mechanical characterization.

Therefore, the objective of this work was to develop and characterize ceramic composites fabricated by direct ink writing, resultant from aqueous based inks comprising a mixture of  $\text{Y}_2\text{O}_3$  and  $\text{Al}_2\text{O}_3$  powders, using CMC and PEI as organic additives. Three-dimensional-printed structures were sintered at different temperatures and the densified bodies characterized by crystallographic and mechanical properties.

## 2. Materials and Methods

Commercial  $\text{Al}_2\text{O}_3$  and  $\text{Y}_2\text{O}_3$  powders were used as raw materials, which main characteristics are presented in Table 1. Homogeneous powder mixture was attained by wet ball milling in ethanol, with alumina spheres at 300 rpm for 72 h. The individual powders and the resultant alumina-yttria mixture were characterized by particle size distribution (LA-960V2, HORIBA Scientific, Kyoto, Japan) and X-ray diffraction, performed in a high-resolution X’Pert PRO diffractometer (Malvern PANalytical, Worcestershire, UK), acquired in a  $2\theta$  range 10–80° with a step size of 0.02°/count (100 s). The identified crystalline phases were quantified by the Rietveld full-pattern fitting method, using the

FullProf Suite program [22]. The crystallographic patterns employed on refinement were obtained from the Inorganic crystal structure database (ICSD).

**Table 1.** Characteristics of the starting  $\text{Al}_2\text{O}_3$  and  $\text{Y}_2\text{O}_3$  powders.

$\text{Al}_2\text{O}_3$ (CT-3000, ALMATIS)		$\text{Y}_2\text{O}_3$ (Fine, H.C.Starck)	
Chemical Composition (%)			
$\text{Al}_2\text{O}_3$	99.8	$\text{Y}_2\text{O}_3$	99.9
$\text{Na}_2\text{O}$	0.03	$\text{Al}_2\text{O}_3$	<0.03
$\text{MgO}$	0.040	$\text{Fe}_2\text{O}_3$	0.015
$\text{SiO}_2 + \text{CaO} + \text{Fe}_2\text{O}_3$	0.045	Ca (ppm)	<0.5
Specific surface area ( $\text{m}^2/\text{g}$ )	7.80		12.8
Density ( $\text{g}/\text{cm}^3$ )	3.98		5.01

### 2.1. Suspension and Paste Preparation

The ink formulation started with the preparation of an aqueous suspension containing approximately 76 wt% (42 vol %) of total amounts of solids and 24 wt% of water by dispersing the powders in deionized water in the presence of 2 wt% (based on the solids amount) of Dolapix CE64 (Zimmer and Schwartz, Lahnstein, Rheinland-Pfalz, Germany), [23,24]. The solids included a mixture of 63.9 wt% aluminium oxide (CT3000-SG, Amaltis GmbH, Ludwigshafen, Germany), 35.9 wt% yttrium oxide (Type-FINE, H.C. Starck, Germany), and 0.2 wt% magnesium oxide (Sigma Aldrich, Darmstadt, Germany). The suspension was then deagglomerated in a ball milling over 24 h. To convert the suspension in a paste with adequate properties for printing, similar types and amounts of additives selected in a previous work for alumina-based inks were used [21,23,24]. Briefly, 0.5 wt% of carboxymethyl cellulose (CMC, 250,000 Mw, Colorobbia, Anadia, Portugal, based on the amounts of total solids in suspension) was added to the suspension with 10-min homogenization at 1000 rpm in a planetary centrifugal mixer (ARE-250, Thinky Co., Tokyo, Japan). Then, 0.2 wt% of polyethyleneimine solution (PEI, Sigma Aldrich, USA, Mn~1800 and Mw~2000, also calculated based on the total amount of solids) was added with subsequent mixing and degassing in the planetary mixer for an additional 5 min at 1100 rpm to ensure high homogeneity.

Suspensions and pastes were characterized by rheological properties using a Kinexus Pro<sup>+</sup> rheometer (Netzsch, Selb, Germany). Flow measurements were evaluated in the shear rate range of 0.1 to 1000  $\text{s}^{-1}$  at room temperature, using a cone-plate system (4 °C/40 mm) with a gap of 150  $\mu\text{m}$ . Final properties of  $\text{Al}_2\text{O}_3$ - $\text{Y}_2\text{O}_3$  paste were recorded by amplitude sweep measurements at 1-Hz frequency in oscillatory mode, using a plate sensor ( $\text{Ø} = 20 \text{ mm}$ ) with 1-mm gap size.

### 2.2. $\text{Al}_2\text{O}_3$ - $\text{Y}_2\text{O}_3$ Samples Preparation by DIW

A DIW system (Model EBDR-A32, 3D Inks, LLC, USA) was used to print cylindrical  $\text{Al}_2\text{O}_3$ - $\text{Y}_2\text{O}_3$  ( $\text{Ø} = 10 \text{ mm}$ ) samples ( $n = 12$ ) with the as-prepared paste as feedstock material. The paste was loaded into a 5-mL syringe (Nordson, Westlake, OH, USA), and extruded from a nozzle with an internal diameter of 0.41 mm with printing velocity of 10 mm/s, layer height of 0.371 mm, and room temperature of 24–27 °C, during printing. The alumina-yttria samples were printed on a smooth alumina substrate at room temperature within a high humidity level (~85% relative humidity). These humidity conditions were assured by using a portable humidifier in the DIW equipment room and controlled by a humidity measuring device. After printing, the samples were dried at room temperature with controlled humidity for 48 h. Figure 1 presents a CAD layer deposition scheme and images of printed and dried samples.

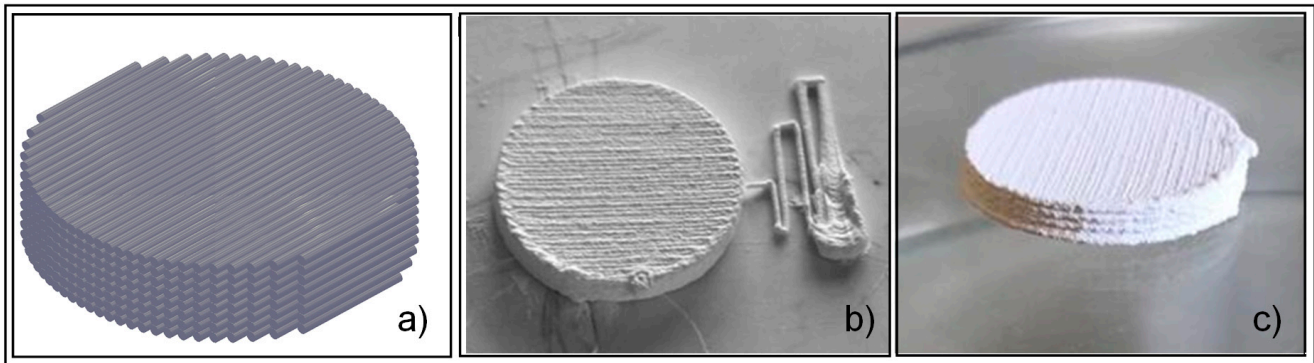


**Figure 1.** (a) Schematic representation of filament layers deposition during 3D building; (b) printed  $\text{Al}_2\text{O}_3\text{-Y}_2\text{O}_3$  sample; (c) after drying for 48 h.

To access the critical temperature for the thermal decomposition of the polymeric additives added on the paste, some dried filaments were submitted to a thermogravimetric analysis (STA300, Hitachi, Japan) with a heating rate of 1 K/min, as presented in Figure 2a. To determine the sintering parameters, a powder mixture, with the same global composition of the paste, was compacted ( $10 \times 4 \times 4$  mm) and subjected to dilatometry tests using a dilatometer (DIL402C, Netzsch, Selb, Germany) with a heating rate of 1 K/min. The shrinkage was measured by linear variable differential transducer (LVDT) with sensitivity of 0.01 mm. After this preliminary dilatometry evaluation (results described in Section 3.2), the printed samples were sintered in a  $\text{MoSi}_2$  furnace by adopting the sintering parameters (heating rates and isothermal dwell times), as highlighted in Figure 2b.

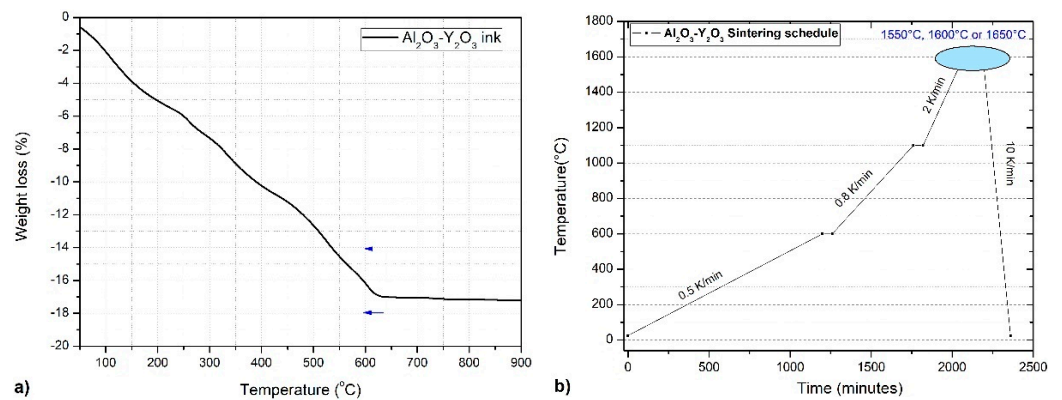


**Figure 2.** (a) Weight loss as function of temperature of the alumina-yttria paste and; (b) Sintering cycle adopted for densification of  $\text{Al}_2\text{O}_3\text{-Y}_2\text{O}_3$  ceramic composites obtained by DIW.

### 2.3. Characterization of Alumina–YAG Printed Samples

Alumina–YAG sintered samples fabricated by DIW were characterized in terms of structural and mechanical performance. Bulk density was obtained by the Archimedes immersion method and relative density was calculated using the mixtures rule by adopting  $3.98 \text{ g}\cdot\text{cm}^{-3}$  as the theoretical density value for  $\text{Al}_2\text{O}_3$  and  $5.46 \text{ g}\cdot\text{cm}^{-3}$  for  $\text{Y}_3\text{Al}_5\text{O}_{12}$  (YAG) crystalline phases, based on quantification accomplished by Rietveld refinement.

Crystalline phases of the sintered samples were evaluated by X-Ray diffraction (XRD) in the same conditions used for the  $\text{Al}_2\text{O}_3\text{-Y}_2\text{O}_3$  powder mixture. The microstructure of the printed and subsequently sintered samples was analyzed in the thermally etched polished surface by scanning electronic microscopy (FEG-SEM SU-70 (Hitachi High-Technologies Europe, GmbH, Krefeld, Germany)). Thermal etching was evaluated by exposing the polished samples at  $1550^\circ\text{C}$  during 15 min with a ramping rate of 20 K/min. Grain size measurements were made using an *Image J* open-source software (National Institute of Mental Health, Bethesda, MD, USA) [25].

Vickers hardness of sintered alumina–YAG samples was measured using polished surfaces. At least 15 indentations were made in each sample with 1 kgf (9.8 N) as the indentation load using a microhardness tester (Wilson VH1102, BUEHLER, Lake Bluff, Illinois, USA) and DiaMet template hardness testing software. Fracture toughness was calculated using the following equation, proposed by Casellas [26]:

$$K_{Ic} = 0.024 \cdot \left( \frac{E}{HV} \right)^{1/2} \cdot \frac{P}{c^{3/2}} \text{ Palmqvist crack model, } 0.25 \leq c/a \leq 2.5 \quad (1)$$

where  $K_{Ic}$  is the fracture toughness [MPa·m<sup>1/2</sup>],  $E$  is the elastic modulus [GPa] = 335 GPa,  $HV$  is the Vickers hardness [GPa],  $P$  is the indentation load [MPa],  $a$  is the semi diagonal of Vickers impression [m], and  $l$  is the crack length [m]; “ $c$ ” = “ $a + l$ ”.

### 3. Results

#### 3.1. Characterization of the Powder’s Mixture and Rheological Behaviour of the Inks

Figure 3 presents the X-ray diffraction results and particle size distribution of the Al<sub>2</sub>O<sub>3</sub>–Y<sub>2</sub>O<sub>3</sub> powder’s mixture. It can be observed that powders mixture exhibited a bimodal distribution, with a highly pronounced group of submicrometric particles with average sizes of 0.15 μm and a second group with average size close to 1.0 μm. Regarding crystalline phases of the mixture, Al<sub>2</sub>O<sub>3</sub> and Y<sub>2</sub>O<sub>3</sub> were only detected, as expected.

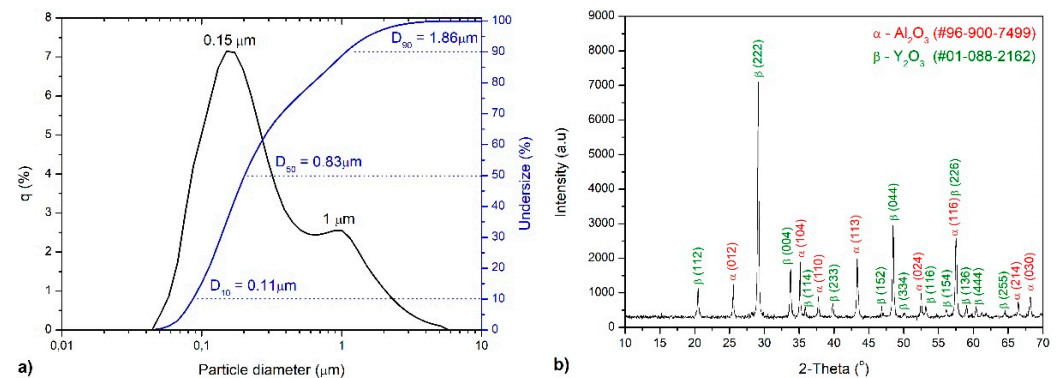


Figure 3. Characterization of the powder’s mixture: (a) particle size distribution; (b) XRD patterns.

Figure 4 shows the results of the rheological study performed on the aqueous-based suspension of Al<sub>2</sub>O<sub>3</sub>–Y<sub>2</sub>O<sub>3</sub> and the respective ink, as a function of the addition of PEI and CMC. Figure 4a presents the viscosity as a function of the shear rate while Figure 4b presents amplitude sweep measurements.

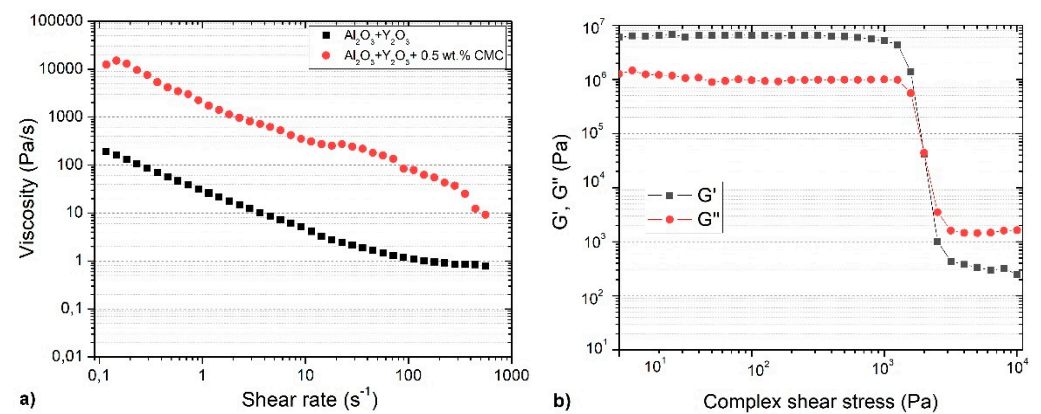
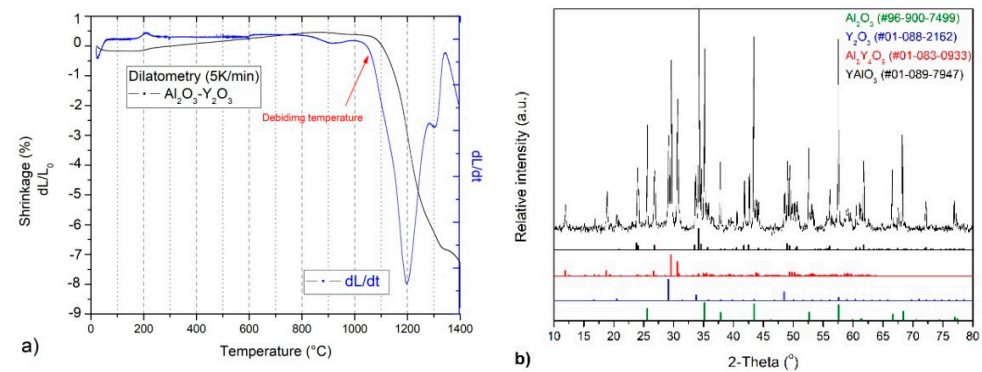


Figure 4. (a) Viscosity versus the shear rate of Al<sub>2</sub>O<sub>3</sub>–Y<sub>2</sub>O<sub>3</sub> suspensions containing 42 vol% of solids in the absence and presence of 0.5 wt% CMC; (b) amplitude sweep of final Al<sub>2</sub>O<sub>3</sub>–Y<sub>2</sub>O<sub>3</sub> ink containing 0.5 wt% CMC and 0.2 wt% PEI.

The  $\text{Al}_2\text{O}_3\text{-Y}_2\text{O}_3$  suspension exhibited shear-thinning behaviour, indicating that it is suitable to go ahead with the printing process. The viscosity of the base suspension increases with the addition of CMC, maintaining the shear-thinning behaviour, as predicted. Figure 4b shows elastic modulus ( $G'$ ) and viscous modulus ( $G''$ ) as a function of the complex shear stress of the final ink (containing both CMC and PEI additives). The paste stays stable over a wide range of applied shear stress (until around  $10^3$  Pa), indicating that the filaments will remain mechanically stable during the printing process with enough strength to support the weight of the successive layers [27,28]. The interception of  $G''$  with  $G'$  means that a rupture of the gel system occurred at shear stress values higher than  $10^3$  Pa, denoting a transition from a solid-like to liquid-like material. Moreover, elastic modulus ( $G'$ ) presents values higher than  $10^6$  Pa, a good indication that the ink presents proper viscoelastic properties for printing.

### 3.2. Thermal Analysis

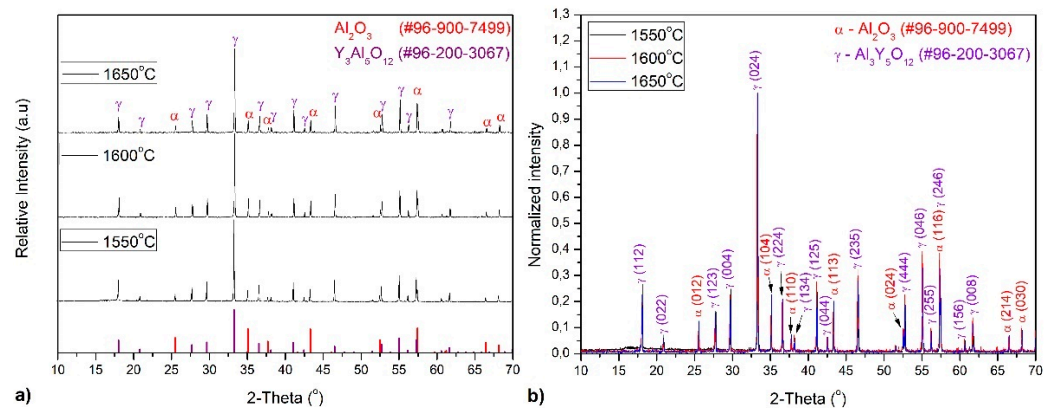
Figure 2a suggests that gravimetric changes are observed only at temperatures up to  $650^\circ\text{C}$ , as attributed to the maximum temperature for the elimination of the polymeric or organic components presented in the initial paste ink. Figure 5 presents dilatometry results of the  $\text{Al}_2\text{O}_3\text{-Y}_2\text{O}_3$  powder-compacted sample. It is possible to identify that the densification process starts at  $1000^\circ\text{C}$  with a maximum shrinkage rate peak observed at  $1200^\circ\text{C}$ . Close to  $1300^\circ\text{C}$ , a slight change in the thermal behavior is also visible (shrinkage profile), which can be probably attributed to the phase transformation reactions in the solid state.  $\text{Al}_2\text{O}_3$  and  $\text{Y}_2\text{O}_3$  are transformed into transient phases, such as  $\text{YAlO}_3$  (YAP) and  $\text{YAl}_{12}\text{O}_9$  (YAM), which subsequently decompose to form the stoichiometric YAG phase ( $\text{Y}_3\text{Al}_5\text{O}_{12}$ ) as the temperature increases [29]. To analyze the crystalline phases presented in the temperature range where the highest shrinkage is observed in the material, a DIW sample was examined after being thermally treated at  $1200^\circ\text{C}$  and the XRD results presented in Figure 5b. The results indicated that  $\text{Al}_2\text{O}_3$  and  $\text{Y}_2\text{O}_3$  were partially converted into the YAP and YAM phases, denoting that, at this temperature, the phenomenon of the phase transformation in the solid state occurred.



**Figure 5.** (a) Dilatometry curve (room temperature  $\rightarrow$   $1400^\circ\text{C}$ ) referring to sintering of optimized  $\text{Al}_2\text{O}_3\text{-Y}_2\text{O}_3$  ceramic ink; (b) XRD pattern of the DIW structure sintered at  $1200^\circ\text{C}$ ; (c) example of a fully sintered sample.

### 3.3. Characterization of the Sintered Samples

Figure 6 presents the X-ray diffraction results of the samples sintered at  $1550^\circ\text{C}$  for 2 h,  $1600^\circ\text{C}$  for 2 h and  $1650^\circ\text{C}$  for 2 h. It can be observed that, in both sintering conditions, only  $\text{Al}_2\text{O}_3$  and  $\text{Y}_3\text{Al}_5\text{O}_{12}$  (YAG) crystalline phases were identified, indicating that  $\text{Y}_2\text{O}_3$  presented in the initial composition. Furthermore, the intermediate phases, YAP and YAM, observed in Figure 5, were completely converted into YAG. Thus,  $\text{Al}_2\text{O}_3\text{-YAG}$  composites containing 53–58 wt% YAG and 42–47 wt%  $\text{Al}_2\text{O}_3$  were obtained after sintering.



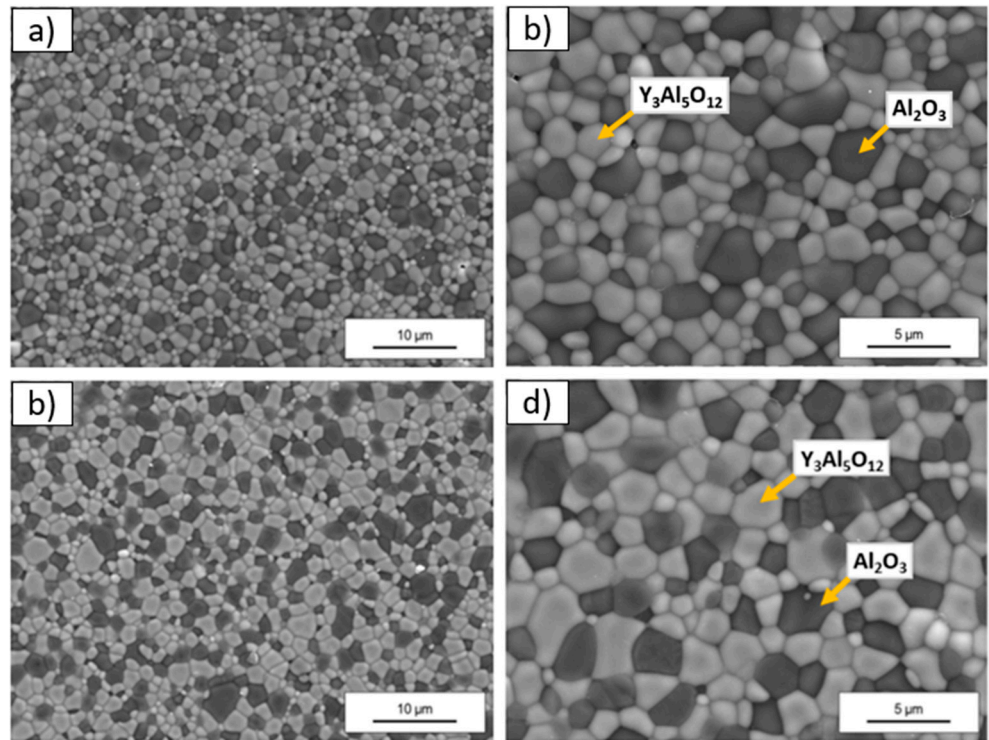
**Figure 6.** (a) XRD patterns of the  $\text{Al}_2\text{O}_3$ –YAG sintered samples at different sintering temperatures (1550 °C, 1600 °C and 1650 °C for 2 h holding time); (b) description of the crystallographic planes of the  $\text{Al}_2\text{O}_3$  and  $\text{Y}_3\text{Al}_5\text{O}_{12}$  phases.

Table 2 presents the results of relative density, Vickers hardness, and fracture toughness of the sintered samples. It is observed that the samples sintered at the lowest temperature (1550 °C) presented average relative density around  $83.7 \pm 0.8\%$  and, consequently, the lowest Vickers hardness values ( $11.6 \pm 0.64$  GPa). The fracture toughness values for these samples are not presented, due to the high imprecision and low accuracy of experimental measurements, related to the high porosity. In contrast, the samples sintered at 1600 °C for 2 h and 1650 °C for 2 h showed satisfactory relative density results for  $\text{Al}_2\text{O}_3$ –based ceramics. The relative density was  $95.4 \pm 0.4\%$  for samples sintered at 1600 °C for 2 h and  $96.5 \pm 0.5\%$  for the ones sintered at 1650 °C for 2 h. The average hardness of the samples obtained at these two sintering conditions were statistically similar, around 14.2 and 14.5 GPa. As sintering temperatures increased, a slight increase in the fracture toughness was observed, with average values of  $3.34 \pm 0.22 \text{ MPa}\cdot\text{m}^{1/2}$  (1600 °C for 2 h) and  $3.54 \pm 0.21 \text{ MPa}\cdot\text{m}^{1/2}$  (1650 °C for 2 h).

**Table 2.** Properties of sintered  $\text{Al}_2\text{O}_3$ –YAG samples obtained by DIW.

Sintering Condition	Relative Density (%)	Hardness (GPa)	<i>cl</i> <i>a</i>	Fracture Toughness ( $\text{MPa}\cdot\text{m}^{1/2}$ )
1550 °C for 2 h	$83.7 \pm 0.8$	$11.6 \pm 0.64$	–	–
1600 °C for 2 h	$95.4 \pm 0.4$	$14.2 \pm 0.27$	$2.21 \pm 0.11$	$3.34 \pm 0.22$
1650 °C for 2 h	$96.5 \pm 0.5$	$14.5 \pm 0.25$	$2.15 \pm 0.09$	$3.54 \pm 0.21$

Figure 7 presents SEM micrographs of the composites sintered at 1600 °C for 2 h and 1650 °C for 2 h, and Figure 8 presents grain size distribution of these ceramic composites. Micrometric grains with average grains sizes of  $1.33 \pm 0.41 \mu\text{m}$  and  $1.13 \pm 0.39 \mu\text{m}$  for  $\text{Al}_2\text{O}_3$  and  $\text{Y}_3\text{Al}_5\text{O}_{12}$ , respectively, were observed in samples sintered at 1600 °C for 2 h, while ceramics sintered at 1650 °C for 2 h present grain size average of  $1.64 \pm 0.53 \mu\text{m}$  ( $\text{Al}_2\text{O}_3$ ) and  $1.46 \pm 0.52 \mu\text{m}$  for the  $\text{Y}_3\text{Al}_5\text{O}_{12}$ , phase, indicating a discrete grain growth of both phases; however, both micrographs can be considered statistically similar. Both crystalline phases are homogeneously well distributed in the volume of the sintered material. This behavior denotes that the mixing and homogenization of the raw materials was successfully attained and subsequently kept in inks preparation for DIW, allowing reactive sintering results in a refined microstructure with well-distributed distinct phases.



**Figure 7.** SEM micrographs of  $\text{Al}_2\text{O}_3$ -YAG composites sintered at: (a) and (b)  $1600\text{ }^\circ\text{C}$  for 2 h; (c) and (d)  $1650\text{ }^\circ\text{C}$  for 2 h.

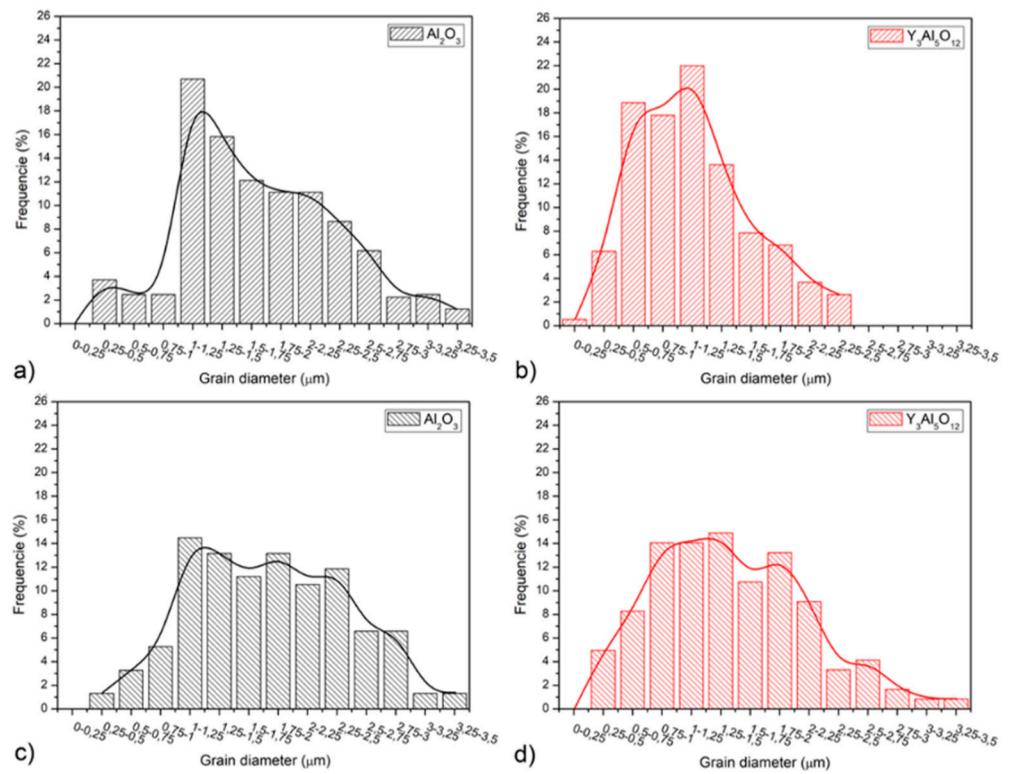


**Figure 8.** Grain size distribution of sintered  $\text{Al}_2\text{O}_3$ -YAG composites: (a) and (c) represent the  $\text{Al}_2\text{O}_3$  grain size distribution for samples sintered at  $1600\text{ }^\circ\text{C}$  for 2 h and  $1650\text{ }^\circ\text{C}$  for 2 h; and (b) and (d) represents the  $\text{Y}_2\text{Al}_5\text{O}_{12}$  grains size distribution for samples sintered at  $1600\text{ }^\circ\text{C}$  for 2h and  $1650\text{ }^\circ\text{C}$  for 2 h.

#### 4. Discussion

The technological updates observed in recent years, regarding the additive manufacturing of ceramic materials, enabled significant advances in microstructural development, densification, and, consequently, the mechanical properties of final materials in general. Low-sinterability ceramics, such as  $\text{Al}_2\text{O}_3$ , require special sintering techniques to obtain high densification. Usually, the complete densification of alumina occurs at temperatures around 1700–1800 °C under a controlled atmosphere and high steeping times. Therefore, exaggerated grain growth as well as increased brittleness are common drawbacks under these processing conditions [30–32]. To decrease the sintering temperature, one of the strategies used to improve the relative density is adding small amounts of MgO in alumina-based composition, which facilitates the diffusion through the grain contours during sintering process [33]. This approach was also adopted in this work. Additionally, by using submicrometric or nanometric powders, the final sintering temperature can also be reduced, keeping the compromise between densification and controlled microstructure (without exaggerated grain growth), resulting in a material with proper hardness and fracture toughness ratio. It is also known that a proper packing behavior between powder mixtures also improves the rheological properties of the suspension, which helps to increase the loading of the solids and, consequently, enhances densification [34,35].

The ink composition used in the present work to fabricate alumina–YAG parts by DIW presents around 42 vol% of solids content, while keeping a shear thinning behavior desirable for printing process (good flow through fine nozzles). Moreover, the high densification attained is a good indication that the ink filaments were also able to fill the void space formed among cylindrical filaments after deposition, without losing the mechanical integrity of the printed structure (as predicted from Figure 1), in good agreement with statements from previous reports [23,28]. Besides inorganic solids, the complementary fraction of the ink is composed of water and organic additives that are eliminated, during drying and sintering processes. In this context, de-binding is a crucial step that should be performed smoothly and gradually to avoid the creation of macroscopic pores, which are difficult to eliminate during thermal treatment. At temperatures below 800 °C, a total elimination of residual water and organic binders was verified in the dilatometry (Figure 5a). A moderate heating rate (0.5 K/min) permitted the gradual and non-aggressive exit of these components, contributing to the high densification of the samples.

The initial stages of the sintering process when shrinkage started to occur are usually characterized by neck formation and the development of open porosity. The composite  $\text{Al}_2\text{O}_3$ – $\text{Y}_2\text{O}_3$  studied in the present work starts above 1070 °C, as shown in Figure 4a. At temperatures between 1200 °C and 1300 °C, it is possible to verify the beginning of the phase transformation process in the solid state, proven by X-ray diffraction performed on the sample sintered at 1200 °C (Figure 5b). As a temperature range where the phenomenon of densification and phase transformations occur simultaneously, it is considered critical for ceramic powder systems containing  $\text{Al}_2\text{O}_3$  and  $\text{Y}_2\text{O}_3$ ; therefore, it should be well understood and controlled. The sintering continuity at higher temperatures leads to the formation of two main phases, namely YAG and  $\text{Al}_2\text{O}_3$ . At the three temperature conditions adopted in this work (1550, 1600, and 1650 °C), the crystalline phases and their respective proportions remained stable (Figure 6). A complete conversion of  $\text{Y}_2\text{O}_3$  into  $\text{Y}_3\text{Al}_5\text{O}_{12}$  by stoichiometric chemical reaction with the  $\text{Al}_2\text{O}_3$  matrix was stated, in good agreement with previous works [14,36,37].

The main difference observed among the three sintering temperatures adopted was the low densification of the robocasted ceramic pieces sintered at 1550 °C for 2 h, perhaps due to the limited sinterability of the  $\text{Al}_2\text{O}_3$  and YAG phases at this temperature. In fact, the 3D structures sintered at this temperature presented high residual porosity (around 16.3%). Whereas, when sintering was carried out at 1600 °C for 2 h or at 1650 °C for 2 h, a considerable gain in densification was noticeable (Table 2). As a consequence of that, an average hardness values of 14.5 GPa and fracture toughness higher than 3.2  $\text{MPa}\cdot\text{m}^{1/2}$  were obtained. The literature reports Vickers hardness values in the range of 11 and

15 GPa and fracture toughness values around 3.0 to 3.5 MPa·m<sup>1/2</sup> [37], for similar powder mixtures (Al<sub>2</sub>O<sub>3</sub>–Y<sub>2</sub>O<sub>3</sub>) processed by conventional manufacturing methods and sintered at temperatures in the range of 1600 and 1650 °C.

Thus, the mechanical properties of the Al<sub>2</sub>O<sub>3</sub>–YAG samples of the current work, consolidated by a new advanced manufacturing technology (direct ink writing and robocasting), are compatible to previous well established processes. Since a ceramic ink containing less than 50 vol% of solids was used, the densification and mechanical performance attained can be attributed to several factors: (i) particle size distribution and morphological characteristics of the Al<sub>2</sub>O<sub>3</sub>–Y<sub>2</sub>O<sub>3</sub> system selected; (ii) an efficient extrudable and homogeneous ceramic ink with proper rheological properties to keep the geometry of the printed structure and concurrently fill the voids between filaments during printing process (prevent connected inter-filament porosity), and (iii) an optimized sintering cycle based on the interpretation of dilatometric studies.

## 5. Conclusions

An extrudable aqueous-based ink containing a mixture of Al<sub>2</sub>O<sub>3</sub>–Y<sub>2</sub>O<sub>3</sub> in a total solid loading of 42 vol% was successfully developed for 3D printing by direct ink writing. Through small amounts of additives (0.5 wt% CMC and 0.2 wt% PEI), it was possible to attain ink with proper rheological performance, i.e., with the ability to flow from a fine nozzle and then fill the inter-filament porosity without losing the final geometry. High-density samples were achieved by the addition of a small amount of MgO in the initial mixture composition, together with the optimization of the sintering step. Three-dimensional structures with high hardness (14.2–14.5 GPa) and fracture toughness (3.34–3.54 MPa·m<sup>1/2</sup>) values were attained by robocasting, which are comparable with the same type of materials fabricated by traditional methods.

**Author Contributions:** Conceptualization, J.B., S.O.; methodology, J.B., M.F.R.P.A., C.d.S.; software, J.B., M.F.R.P.A.; validation, C.d.S., S.O.; formal analysis, J.B., M.F.R.P.A.; investigation, J.B., C.d.S.; resources, J.B.; data curation, J.B., M.F.R.P.A., C.d.S.; writing—original J.B., C.d.S.; draft preparation, J.B., M.F.R.P.A.; writing—review and editing, C.d.S., S.O.; visualization, C.d.S., S.O.; supervision, S.O.; project administration, C.d.S., S.O.; funding acquisition, C.d.S., S.O. All authors have read and agreed to the published version of the manuscript.

**Funding:** This research was funded by FCT-Fundação para a Ciência e Tecnologia, Portugal, grant number CEECIND/03393/2017; and FAPERJ-Fundação Carlos Chagas de Ciência e Tecnologia do estado do Rio de Janeiro, Brazil, grant number E-26-201.476/2014 and E26-202.997/2017.

**Institutional Review Board Statement:** Not applicable.

**Informed Consent Statement:** Not applicable.

**Acknowledgments:** This work was supported by the project “TAMAZ3D—Development of a Decision Support Tool for Additive Manufacturing of Alumina-Zirconia 3-D structures” (POCI-01-0145-FEDER-030493). This work was also supported by the projects of CICECO (UIDB/50011/2020 & UIDP/50011/2020) and TEMA (UID/EMS/00481/2020), all financed by national funds through the FCT/MEC and when appropriate co-financed by the European Regional Development Fund (ERDF) under the PT2020 Partnership Agreement. S. M. Olhero acknowledge Portuguese Foundation for Science and Technology (FCT) for CEECIND/03393/2017 contract.

**Conflicts of Interest:** The authors declare no conflict of interest.

## References

1. Dörre, E.; Hubner, H. *Alumina: Processing, Properties, and Applications*; Springer: Berlin, Germany, 1984; ISBN 3540135766/9783540135760.
2. Ruys, A.J. *Alumina Ceramics: Biomedical and Clinical Applications*; Woodhead Publishing: Oxford, UK, 2019.
3. Prathumwan, R.; Subannajui, K. Fabrication of a ceramic/metal (Al<sub>2</sub>O<sub>3</sub>/Al) composite by 3D printing as an advanced refractory with enhanced electrical conductivity. *RSC Adv.* **2020**, *10*, 32301–32308. [[CrossRef](#)]
4. Chakravarty, D.; Bysakh, S.; Muraleedharan, K.; Rao, T.N.; Sundaresan, R. Spark plasma sintering of magnesia-doped alumina with high hardness and fracture toughness. *J. Am. Ceram. Soc.* **2008**, *91*, 203–208. [[CrossRef](#)]

5. Yang, S.; Yang, S.; Zhu, Y.; Fan, L.; Zhang, M. Flash Sintering of dense alumina ceramic discs with high hardness. *J. Eur. Ceram. Soc.* **2022**, *42*, 202–206. [[CrossRef](#)]
6. Xia, Z.; Li, L. Understanding interfaces and mechanical properties of ceramic matrix composites. *Adv. Ceram. Matrix Compos.* **2014**, *1*, 267–285. [[CrossRef](#)]
7. Sommer, F.; Landfried, R.; Kern, F.; Gadow, R. Mechanical properties of zirconia toughened alumina with 10–24 vol% 1.5 mol% Y-TZP reinforcement. *J. Eur. Ceram. Soc.* **2012**, *32*, 3905–3910. [[CrossRef](#)]
8. Zadorozhnaya, O.Y.; Khabas, T.A.; Kamyshnaya, K.S.; Kutugin, V.A.; Malykhin, S.E. Effects of sintering curves on microstructure, physical and mechanical properties and on low temperature degradation of zirconia-toughened alumina. *J. Eur. Ceram. Soc.* **2021**, *41*, 274–281. [[CrossRef](#)]
9. Korte, C.; Franz, B. Reaction kinetics in the system  $Y_2O_3/Al_2O_3$ —A solid state reaction forming multiple product phases investigated by using thin film techniques. *Solid State Ionics* **2021**, *368*, 115699. [[CrossRef](#)]
10. Liu, B.; Li, J.; Ivanov, M.; Liu, W.; Liu, J.; Xie, T.; Zhuo, S.; Pan, Y.; Guo, J. Solid-state reactive sintering of Nd:YAG transparent ceramics: The effect of  $Y_2O_3$  powders pretreatment. *Opt. Mater.* **2014**, *9*, 1591–1597. [[CrossRef](#)]
11. Mah, T.; Parthasarathy, T.A.; Matson, L.E. Processing and Mechanical Properties of  $Al_2O_3/Y_3Al_5O_{12}$  (YAG) Eutectic Composite. *Ceram. Eng. Sci. Proc.* **1990**, *11*, 1617–1627. [[CrossRef](#)]
12. Yoshida, H.; Nakamura, A.; Sakuma, T.; Nakagawa, N.; Waku, Y. Anisotropy in high-temperature deformation in unidirectionally solidified eutectic  $Al_2O_3$ –YAG single crystals. *Scr. Mater.* **2001**, *45*, 957–963. [[CrossRef](#)]
13. Ochiai, S.; Ueda, T.; Sato, K.; Hojo, M.; Waku, Y.; Nakagawa, N.; Sakata, S.; Mitani, A.; Takahashi, T. Deformation and fracture behavior of an  $Al_2O_3$ /YAG composite from room temperature to 2023 K. *Compos. Sci. Technol.* **2001**, *61*, 2117–2128. [[CrossRef](#)]
14. Paneto, F.J.; Pereira, J.L.; Lima, J.O.; Jesus, E.J.; Silva, L.A.; Sousa Lima, E.; Cabral, R.F.; Santos, C. Effect of porosity on hardness of  $Al_2O_3$ – $Y_3Al_5O_{12}$  ceramic composite. *Int. J. Refract. Met. Hard Mater.* **2015**, *48*, 365–368. [[CrossRef](#)]
15. Peng, E.; Zhang, D.; Ding, J. Ceramic Robocasting: Recent Achievements, Potential, and Future Developments. *Adv. Mater.* **2018**, *30*, 1–14. [[CrossRef](#)]
16. Fu, Z.; Freihart, M.; Wahl, L.; Fey, T.; Greil, P.; Travitzky, N. Micro- and macroscopic design of alumina ceramics by robocasting. *J. Eur. Ceram. Soc.* **2017**, *37*, 3115–3124. [[CrossRef](#)]
17. Lakhdar, Y.; Tuck, C.; Binner, J.; Terry, A.; Goodridge, R. Additive manufacturing of advanced ceramic materials. *Prog. Mater. Sci.* **2021**, *116*, 100–736. [[CrossRef](#)]
18. Rueschhoff, L.; Costakis, W.; Michie, M.; Youngblood, J.; Trice, R. Additive Manufacturing of Dense Ceramic Parts via Direct Ink Writing of Aqueous Alumina Suspensions. *Int. J. Appl. Ceram. Technol.* **2016**, *13*, 821–830. [[CrossRef](#)]
19. Scheithauer, U.; Schwarzer, E.; Richter, H.J.; Moritz, T. Thermoplastic 3D printing—An additive manufacturing method for producing dense ceramics. *Int. J. Appl. Ceram. Technol.* **2015**, *12*, 26–31. [[CrossRef](#)]
20. Schlordt, T.; Schwanke, S.; Keppner, F.; Fey, T.; Travitzky, N.; Greil, P. Robocasting of alumina hollow filament lattice structures. *J. Eur. Ceram. Soc.* **2013**, *33*, 3243–3248. [[CrossRef](#)]
21. Zhang, G.; Carloni, D.; Wu, Y. 3D printing of transparent YAG ceramics using copolymer-assisted slurry. *Ceram. Int.* **2020**, *46*, 17130–17134. [[CrossRef](#)]
22. Rodriguez-Carvajal, J. FULLPROF: A Program for Rietveld Refinement and Pattern Matching Analysis. In *Abstracts of the Satellite Meeting on Powder Diffraction of the XV Congress of the IUCr*; International Union of Crystallography (IUCr): Toulouse, France, 1990; p. 127.
23. Baltazar, J.; Torres, P.M.C.; Dias-de-Oliveira, J.; Pinho-da-Cruz, J.; Gouveia, S.; Olhero, S. Influence of filament patterning in structural properties of dense alumina ceramics printed by robocasting. *J. Manuf. Process.* **2021**, *68*, 569–582. [[CrossRef](#)]
24. Ganesh, I.; Sundararajan, G.; Olhero, S.M.; Torres, P.M.C.; Ferreira, J.M.F. A novel colloidal processing route to alumina ceramics. *Ceram. Int.* **2010**, *36*, 1357–1364. [[CrossRef](#)]
25. Lau, M.; Morgenstern, F.; Hübscher, R.; Knospe, A.; Herrmann, M.; Döring, M.; Lippmann, W. Image Segmentation Variants for Semi-Automated Quantitative Microstructural Analysis with ImageJ. *Pract. Metallogr.* **2020**, *57*, 752–775. [[CrossRef](#)]
26. Casellas, D.; Ràfols, I.; Llanes, L.; Anglada, M. Fracture toughness of zirconia–alumina composites. *Int. J. Refract. Met. Hard Mater.* **1999**, *17*, 11–20. [[CrossRef](#)]
27. Nan, B.; Olhero, S.; Pinho, R.; Vilarinho, P.M.; Button, T.W.; Ferreira, J.M.F. Direct ink writing of macroporous lead-free piezoelectric  $Ba_{0.85}Ca_{0.15}Zr_{0.1}Ti_{0.9}O_3$ . *J. Am. Ceram. Soc.* **2019**, *102*, 3191–3203. [[CrossRef](#)]
28. M'Barki, A.; Bocquet, L.; Stevenson, A. Linking Rheology and Printability for Dense and Strong Ceramics by Direct Ink Writing. *Sci. Rep.* **2017**, *7*, 1–10. [[CrossRef](#)]
29. Abell, J.S.; Harris, I.R.; Cockayne, B.; Lent, B. An investigation of phase stability in the  $Y_2O_3$ – $Al_2O_3$  system. *J. Mater. Sci.* **1974**, *9*, 527–537. [[CrossRef](#)]
30. Maca, K.; Pouchlý, V.; Bodišová, K.; Švančárek, P.; Galusek, D. Densification of fine-grained alumina ceramics doped by magnesia, yttria and zirconia evaluated by two different sintering models. *J. Eur. Ceram. Soc.* **2014**, *34*, 4363–4372. [[CrossRef](#)]
31. Miranzo, P.; Taberner, L.; Moya, J.S.; Jurado, J.R. Effect of Sintering Atmosphere on the Densification and Electrical Properties of Alumina. *J. Am. Ceram. Soc.* **1990**, *73*, 2119–2121. [[CrossRef](#)]
32. Zhang, X.; Liang, S.; Zhang, P.; Zhao, T.; Bai, Y.; Bao, C.G.; Yang, J.F.; Qiao, G.J. Fabrication of Transparent Alumina by Rapid Vacuum Pressureless Sintering Technology. *J. Am. Ceram. Soc.* **2012**, *95*, 2116–2119. [[CrossRef](#)]

33. Mamoun, A.; Epicier, T.; Gros, H.; Fantozzi, G. Microstructural study of a MgO-doped alumina-based ceramic. *Mater. Chem. Phys.* **1992**, *32*, 169–176. [[CrossRef](#)]
34. Olhero, S.M.; Ganesh, I.; Torres, P.M.C.; Alves, F.J.; Ferreira, J.M.F. Aqueous colloidal processing of ZTA composites. *J. Am. Ceram. Soc.* **2009**, *92*, 9–16. [[CrossRef](#)]
35. Olhero, S.M.; Ferreira, J.M.F. Influence of particle size distribution on rheology and particle packing of silica-based suspensions. *Powder Technol.* **2004**, *139*, 69–75. [[CrossRef](#)]
36. De Souza Lima, E.; Louro, L.H.L.; De Freitas Cabral, R.; De Campos, J.B.; De Avillez, R.R.; Da Costa, C.A. Processing and characterization of Al<sub>2</sub>O<sub>3</sub>-yttrium aluminum garnet powders. *J. Mater. Res. Technol.* **2013**, *2*, 18–23. [[CrossRef](#)]
37. Lima, E.S.; Itaboray, L.M.; Santos, A.P.O.; Santos, C.; Cabral, R.F. Mechanical Properties Evaluation of Al<sub>2</sub>O<sub>3</sub>-YAG Ceramic Composites. *Mater. Sci. Forum* **2015**, *820*, 239–243. [[CrossRef](#)]